

# Low-Rank Acceleration of the Operator Fourier Transform

Jack Kelley<sup>†</sup>

*Project advisor: Daniel Appelo<sup>‡</sup>*

---

**Abstract.** We develop a numerical algorithm for the efficient solution or approximation of solutions to the Helmholtz equation on a structured grid in two dimensions. We make use of the Operator Fourier Transform (OFT) and a low-rank cross approximation scheme (Cross-DEIM) to decompose the problem into an integral over a pseudo-time of solutions to the Schrödinger equation. The OFT is a framework for solving operator equations like fractional Laplacian equations or the Helmholtz equation, when the latter is written as a product of two paraxial operators. The main computational cost in the OFT is the solution to the Schrödinger equation, especially when the dimension or mesh resolution is high. In this work, we alleviate this cost by utilizing a low-rank method. Such methods aim to beat the curse of dimensionality when low-rank structures are present in the solution. We show that the combination of these two approaches can have large cost reductions for certain classes of problems.

**1. Introduction.** The study of waves arises in many science and engineering applications. Waves are able to carry information over a distance, enabling both natural (through animal sonar and speech) and technological communication [10]. Waves also underpin various imaging and probing methods, either through direct reception (eyes, cameras) or by solving an inverse problem as in, for example, computed tomography [3]. It is therefore necessary to develop fast and robust methods for computing the solution to problems involving waves. In this paper we are interested in solving the Helmholtz equation, which is the time-independent version of the wave equation.

We present an adaptation of the Operator Fourier Transform (OFT) [4] that makes use of the Cross-DEIM algorithm proposed in [1] for the low-rank solution of the Helmholtz equation. The specific formulation of the Helmholtz equation that we will use is

$$(1.1) \quad \begin{aligned} m(\mathbf{x})v(\mathbf{x}) + \frac{1}{\kappa^2}\Delta v(\mathbf{x}) &= g(\mathbf{x}), & \mathbf{x} \in \Omega, \\ v(\mathbf{x}) &= 0, & \mathbf{x} \in \partial\Omega, \end{aligned}$$

where  $\kappa$  is the wavenumber,  $m$  is the index of refraction,  $\mathbf{x} \in \Omega \subset \mathbb{R}^d$  where  $d$  is the dimension.  $\Delta v(\mathbf{x})$  denotes the Laplacian of  $v(\mathbf{x})$ . The use of the OFT for the Helmholtz equation was first motivated by the difficulty with obtaining a numerical solution with iterative methods. In comparison, the OFT framework leads to the implementation of a direct solver where the Helmholtz operator is inverted via the solution of two time-dependent linear Schrödinger equations. These solutions are then summed within a Fourier integral over a time-like variable  $\tau$ .

The OFT framework allows for any method to be used for the evaluation of the Schrödinger equation. We choose to use low-rank methods to compute an approximation to the solution

---

<sup>†</sup>Computational Modeling and Data Analytics Program, Virginia Tech ([jackkelley@vt.edu](mailto:jackkelley@vt.edu)).

<sup>‡</sup>Department of Mathematics, Virginia Tech ([appelo@vt.edu](mailto:appelo@vt.edu)).

of the Schrödinger equation. As described in [11], the Schrödinger equation has a long history of being evaluated on low-rank manifolds, stretching back to Dirac in the 1930s [6]. It is demonstrated in Section II of [12] that for the Schrödinger equation, when a large system is approximated by a low-rank representation, the error is bounded by the best-approximation error of the Schrödinger solution on to the low-rank manifold.

The goal of low-rank methods is to exploit a low-rank structure present in the solution. On a grid in two dimensions the discrete solution can be represented by the matrix  $X \in \mathbb{C}^{m \times n}$  where the entry  $X_{ij}$  approximates the solution at the grid point  $(x_i, y_j)$ . We write  $X = V + iW$  with  $V, W \in \mathbb{R}^{m \times n}$ , as detailed in section 3, and approximate both  $V$  and  $W$  as a rank  $r$  matrix, where  $r \ll \min(m, n)$ . This allows us to only store and evaluate part of the solution, reducing both the memory footprint and the number of operations required for a solution. Low-rank acceleration is a natural extension of the OFT, as the primary computational cost of the evaluation of the OFT integral is the solution to the Schrödinger equation. Using the Cross-DEIM algorithm our method is able to scale in two dimensions as  $O((m+n)r^2)$ .

To advance  $V$  and  $W$  in time we introduce a new scheme making use of this real-imaginary splitting. We employ an exponential time-stepping scheme developed in [4] in which the initial and final step sizes are prescribed and the intermediate nodes grow geometrically; this is well-suited to the OFT integrand, whose decay in  $\tau$  allows larger steps at later times without significant loss of accuracy. At each step we apply a midpoint discretization and diagonalize the discrete Laplacian via a discrete sine transform, and in this basis the coupled update for  $\hat{V}$  and  $\hat{W}$  decouples pointwise. The time step then reduces, at each grid point  $(i, j)$ , to multiplication by a  $2 \times 2$  rotation matrix with angle  $\theta$  and prefactor  $\phi$  determined by the local index of refraction. When the medium is non-absorbing,  $\phi = 1$  and the scheme is norm-preserving; otherwise  $\phi < 1$  leads to dissipation.

The low-rank algorithm we choose to use is Cross-DEIM, as developed in [1]. We choose to use this algorithm as it does not require us to ever form the full matrices used in our Schrödinger solver, keeping all intermediate steps low-rank. The Cross-DEIM algorithm is an iterative greedy method that finds a low rank approximation in SVD form of a matrix  $G$ , without requiring access to the full matrix. Given a set of row indices  $I$  and column indices  $J$  of the matrix  $G$  we approximate  $G$  as

$$(1.2) \quad G \approx G(:, I)UG(J, :)$$

where  $G(:, I)$  denotes the submatrix of  $G$  formed by all rows and the columns indexed by  $I$ , and  $G(J, :)$  denotes the rows indexed by  $J$  and all columns. This is similar to the CUR decomposition, however, instead of  $U = G(:, J)^\dagger G G(I, :)$  as in the CUR decomposition [13], we choose  $U = G(I, J)^\dagger$ . This choice of  $U$  is more efficient than in the traditional CUR decomposition as we do not need to have access to the full matrix  $G$ , and we compute only one pseudoinverse as opposed to two. The algorithms for selecting the optimal index sets  $I$  and  $J$  are expanded upon in subsection 4.2. One advantage of using Cross-DEIM is that it is rank adaptive, i.e. it is possible to prescribe a certain error tolerance and the rank of the solution will adapt at each time step to keep the solution within the level of allowed error. Cross-DEIM builds off of ideas developed in [9] that allow a reconstruction of an  $m \times n$  matrix with  $r$  rows and columns with a pseudo-skeleton approximation. This method is extended to

tensors in [14] and a Cross<sup>2</sup>-DEIM algorithm has been developed in [2], however this paper deals only with the two-dimensional case.

The rest of this paper is organized as follows. We give an overview of the OFT in section 2 and an overview of our low-rank solver in section 3. We show experimental results in section 5, and our conclusions are in section 6.

**2. Operator Fourier Transform.** Following [4], the OFT is defined as a function  $f$  on a general operator  $A$ , applied to another function  $g$ :

$$(2.1) \quad [f(A)g](\mathbf{x}) = \frac{1}{\sqrt{2\pi}} \int_0^\infty \hat{f}(\tau) e^{i\tau A} g(\mathbf{x}) dt.$$

In this formulation,  $f$  is a function of both an operator and a spatial vector,  $g$  is a function of a spatial vector, and  $\hat{f}$  is the Fourier transform of  $f$ . It is then possible to evaluate the term  $u := e^{itA}g(\mathbf{x})$  by solving the system of differential equations.

$$(2.2) \quad \begin{aligned} u_t(t, \mathbf{x}) &= iAu(t, \mathbf{x}), \\ u(0, \mathbf{x}) &= g(\mathbf{x}), \end{aligned}$$

which in this work is done with a low-rank method. Using the OFT framework the problem of inverting the operator is reduced to first solving  $u_t(\tau, \mathbf{x}) = iAu(\tau, \mathbf{x})$  and then using that solution in the Fourier integral time step. We can expect to be able to quickly approximate the integral when  $\hat{f}$  decays quickly in  $\tau$ .

**2.1. Using the OFT to solve an ODE.** Before we begin using the OFT to solve (1.1), we revisit this simple example from [4]. Consider the ODE

$$(2.3) \quad v(x) - iv_{xx}(x) = g(x).$$

To use the OFT to solve this equation, we let  $A = \partial_{xx}$ , then writing (2.3) as

$$(2.4) \quad v(x)(I - iA) = g(x),$$

we see that

$$(2.5) \quad v(x) = (I - iA)^{-1} g(x).$$

Defining  $f(A) := (I - iA)^{-1}$ , we can write the solution as

$$(2.6) \quad v(x) = [f(A)g](x) = \frac{1}{\sqrt{2\pi}} \int_0^\infty e^{-\tau} e^{i\tau A} g(x) d\tau$$

where  $\hat{f}(\tau) = \sqrt{2\pi}e^{-\tau}H(\tau)$  is the Fourier transform of  $f$  and  $H(\tau)$  is the Heaviside function. The solution to the specific IBVP (2.2) can then be inserted into (2.6), which can in turn be evaluated with a numerical integration scheme.

**2.2. Using the OFT to solve the Helmholtz equation.** As our objective is to find the solution to the Helmholtz equation, we must first formulate a Helmholtz operator in order to treat it with the OFT. To do this, Cubillos and Jimenez in [4] define

$$(2.7) \quad A = m(x) + \frac{\Delta}{\kappa^2}$$

and, since the Fourier transform of  $f(x) = x^{-\frac{1}{2}}$  is

$$(2.8) \quad \hat{f}(\tau) = \sqrt{\frac{-i}{\pi}} H(\tau) \frac{1}{\sqrt{\tau}},$$

we can write the inverse square root Helmholtz operator as

$$(2.9) \quad f(A) = \sqrt{\frac{-i}{\pi}} \int_0^\infty \frac{e^{i\tau}}{\sqrt{\tau}} e^{i\tau(A-I)} d\tau.$$

To find the solution to the Helmholtz equation (1.1) we apply  $f(A)$  to  $g$  twice,

$$(2.10) \quad \tilde{v} = f(A)g = \sqrt{\frac{-i}{\pi}} \int_0^\infty \frac{e^{i\tau}}{\sqrt{\tau}} e^{i\tau(A-I)} g(x) d\tau$$

followed by

$$(2.11) \quad v = f(A)\tilde{v} = \sqrt{\frac{-i}{\pi}} \int_0^\infty \frac{e^{i\tau}}{\sqrt{\tau}} e^{i\tau(A-I)} \tilde{v}(x) d\tau.$$

**2.3. Numerical integration of the OFT integral.** To demonstrate one way to numerically integrate the action of  $f(A)$  on  $g$ , we will closely follow [4] and make use of an exponential time stepping scheme and the same quadrature weights. The exponential time stepping scheme evaluates the Fourier integral at the times

$$(2.12) \quad t_n = a(b^n - 1)$$

where  $n$  is the step number,  $n \geq 1$ . It is then possible to proscribe the time step size at the first step  $t_0$  and the last step  $t_f$  of the integration,  $\Delta t_0$  and  $\Delta t_f$  respectively. We therefore choose the two variables  $a$  and  $b$  to satisfy

$$(2.13) \quad a = \frac{t_f}{R}, \quad b = 1 + \frac{R\Delta t_0}{t_f}, \quad R = \frac{\Delta t_f}{\Delta t_0} - 1.$$

Following from [4], with  $u(x, t) = e^{it(A-I)}g(x)$  we can write (2.10) as

$$(2.14) \quad \sqrt{\frac{-i}{\pi}} \int_0^\infty \frac{e^{it}}{\sqrt{t}} u(x, t) dt = \sum_{n=1}^N w_n u_n$$

for  $w_n$  given as

$$(2.15) \quad \begin{aligned} w_1(0, t_1), & \quad n = 0, \\ \omega_n = w_2(t_{n-1}, t_n) + w_1(t_n, t_{n+1}), & \quad 1 \leq n \leq N-1, \\ w_2(t_{N-1}, t_N), & \quad n = N, \end{aligned}$$

$$(2.16) \quad w_1(a, b) = \frac{1+i}{\sqrt{2\pi}(b-a)} \left[ \sqrt{b} e^{ib} - \sqrt{a} e^{ia} + (1+2ib)(C(\sqrt{a}) - C(\sqrt{b}) + iS(\sqrt{a}) - iS(\sqrt{b})) \right],$$

$$(2.17) \quad w_2(a, b) = \frac{1+i}{\sqrt{2\pi}(b-a)} \left[ \sqrt{a} e^{ia} - \sqrt{b} e^{ib} + (1+2ia)(C(\sqrt{b}) - C(\sqrt{a}) + iS(\sqrt{b}) - iS(\sqrt{a})) \right],$$

where

$$(2.18) \quad S(x) = \int_0^x \sin(t^2) dt, \quad C(x) = \int_0^x \cos(t^2) dt.$$

**3. Method for finding an approximation to the solution of the Schrödinger equation.** To evaluate (2.10) and (2.11) we must first develop a method to evaluate  $X(\mathbf{x}, t) = e^{it(A-I)}g(\mathbf{x})$ . We therefore design a low-rank scheme to evaluate equations of the form

$$(3.1) \quad \begin{aligned} X_t &= i \left( (m(\mathbf{x}) - 1) X + \frac{\Delta}{\kappa^2} X \right), & \mathbf{x} \in \Omega, \\ X(\mathbf{x}, t) &= 0, & \mathbf{x} \in \partial\Omega, \\ X(\mathbf{x}, 0) &= g(\mathbf{x}), & \mathbf{x} \in \Omega. \end{aligned}$$

where  $\Delta$  is the Laplacian operator. The index of refraction  $m(\mathbf{x})$  is in general complex-valued, with the real part governing wave propagation and the imaginary part accounting for absorption in the medium. We therefore write  $m(\mathbf{x}) - 1 = \alpha(\mathbf{x}) + i\beta(\mathbf{x})$ , where  $\alpha(\mathbf{x}) \in \mathbb{R}$  governs the oscillatory motion and  $\beta(\mathbf{x}) \geq 0$  describes the level of absorption. Equation (3.1) then becomes

$$(3.2) \quad X_t = i \left( \alpha + \frac{\Delta}{\kappa^2} \right) X - \beta X.$$

We then write  $X = V + iW$  with  $V, W \in \mathbb{R}$ . Substituting into (3.2) and equating real and imaginary parts yields

$$(3.3) \quad \begin{aligned} V_t &= - \left( \alpha + \frac{\Delta}{\kappa^2} \right) W - \beta V, \\ W_t &= \left( \alpha + \frac{\Delta}{\kappa^2} \right) V - \beta W. \end{aligned}$$

In this form,  $\beta$  acts as a damping term on each component, while  $\alpha + \Delta/\kappa^2$  describes the coupling between  $V$  and  $W$ .

**3.1. Discretization on a Cartesian grid.** To approximate the solution of (3.3) numerically we take  $\Omega = [0, 1]^2$  and discretize it with a uniform Cartesian grid of  $(n + 2) \times (n + 2)$  points

$$(3.4) \quad x_i = ih, \quad y_j = jh, \quad 0 \leq i, j \leq n + 1, \quad h = \frac{1}{n + 1},$$

where  $h$  is the spacing between adjacent grid points in both directions. The boundary  $\partial\Omega$  corresponds to the indices  $i \in \{0, n + 1\}$  and  $j \in \{0, n + 1\}$ , leaving the  $n \times n$  interior points  $(x_i, y_j)$ ,  $1 \leq i, j \leq n$ , as the unknowns of the discrete problem.

On this grid we introduce the real-valued grid functions

$$(3.5) \quad V_{ij}(t) \approx V(x_i, y_j, t), \quad W_{ij}(t) \approx W(x_i, y_j, t),$$

and assemble them into  $n \times n$  matrices  $V(t), W(t) \in \mathbb{R}^{n \times n}$  with entries  $V_{ij}, W_{ij}$ . The homogeneous Dirichlet condition  $X = 0$  on  $\partial\Omega$  enforces  $V_{0,j} = V_{n+1,j} = V_{i,0} = V_{i,n+1} = 0$  and likewise for  $W$ , so the boundary values do not appear as unknowns.

Following the standard centered-difference approximation [5, §6.3], the one-dimensional second derivative is approximated at an interior point  $x_i$  by

$$(3.6) \quad -\frac{d^2V}{dx^2}\Big|_{x=x_i} \approx \frac{2V_i - V_{i-1} - V_{i+1}}{h^2}.$$

Collecting these approximations for  $i = 1, \dots, n$  and using the Dirichlet boundary values  $V_0 = V_{n+1} = 0$  gives the symmetric positive-definite tridiagonal matrix

$$(3.7) \quad T_n = \begin{bmatrix} 2 & -1 & & & \\ -1 & 2 & -1 & & \\ & -1 & \ddots & \ddots & \\ & & \ddots & \ddots & -1 \\ & & & -1 & 2 \end{bmatrix} \in \mathbb{R}^{n \times n},$$

so that  $-d^2/dx^2 \approx h^{-2}T_n$  in the discrete setting. In two dimensions, applying (3.6) along each coordinate direction yields the standard five-point stencil approximation [5, §6.3.2]

$$(3.8) \quad -\Delta V|_{(x_i, y_j)} \approx \frac{1}{h^2}(T_n V + V T_n)_{ij},$$

so the discrete Laplacian acts on the matrix of unknowns directly. The matrix  $T_n$  has the eigendecomposition

$$(3.9) \quad T_n = Z\Lambda Z^T, \quad \Lambda = \text{diag}(\lambda_1, \dots, \lambda_n), \quad \lambda_k = 2 \left(1 - \cos \frac{k\pi}{n + 1}\right),$$

with orthonormal eigenvectors  $Z_{ik} = \sqrt{2/(n + 1)} \sin(ik\pi/(n + 1))$  [5, Lemma 6.1], so  $Z$  and  $Z^T$  can be applied in  $O(n \log n)$  operations via the discrete sine transform (DST).

We discretize (3.3) in time using the midpoint rule. With  $V^n, W^n$  the grid-function matrices at time  $t^n$ , define

$$(3.10) \quad \bar{V} = \frac{1}{2}(V^{n+1} + V^n), \quad \bar{W} = \frac{1}{2}(W^{n+1} + W^n),$$

so that, using (3.8) to discretize  $\Delta$ ,

$$(3.11) \quad \begin{aligned} \frac{V^{n+1} - V^n}{\Delta t} &= - \left( \alpha \bar{W} - \frac{1}{h^2 \kappa^2} (T_n \bar{W} + \bar{W} T_n) \right) - \beta \bar{V}, \\ \frac{W^{n+1} - W^n}{\Delta t} &= \left( \alpha \bar{V} - \frac{1}{h^2 \kappa^2} (T_n \bar{V} + \bar{V} T_n) \right) - \beta \bar{W}. \end{aligned}$$

Using the eigendecomposition (3.9) we apply  $Z$  and  $Z^T$  via the DST and rewrite

$$(3.12) \quad \begin{aligned} V^{n+1} - V^n &= \Delta t \left( -\alpha \bar{W} + \frac{1}{h^2 \kappa^2} (Z \Lambda Z^T \bar{W} + \bar{W} Z \Lambda Z^T) - \beta \bar{V} \right), \\ W^{n+1} - W^n &= \Delta t \left( \alpha \bar{V} - \frac{1}{h^2 \kappa^2} (Z \Lambda Z^T \bar{V} + \bar{V} Z \Lambda Z^T) - \beta \bar{W} \right). \end{aligned}$$

With the identifications

$$(3.13) \quad V^{n+1} - V^n = 2\bar{V} - 2V^n, \quad W^{n+1} - W^n = 2\bar{W} - 2W^n,$$

and defining the transformed quantities

$$(3.14) \quad \hat{V} = Z^T \bar{V} Z, \quad \hat{V}^n = Z^T V^n Z, \quad \hat{W} = Z^T \bar{W} Z, \quad \hat{W}^n = Z^T W^n Z,$$

the system decouples as

$$(3.15) \quad \begin{aligned} \hat{V} - \hat{V}^n &= \frac{\Delta t}{2} \left( -\alpha \hat{W} + \frac{1}{h^2 \kappa^2} (\Lambda \hat{W} + \hat{W} \Lambda) - \beta \hat{V} \right), \\ \hat{W} - \hat{W}^n &= \frac{\Delta t}{2} \left( \alpha \hat{V} - \frac{1}{h^2 \kappa^2} (\Lambda \hat{V} + \hat{V} \Lambda) - \beta \hat{W} \right). \end{aligned}$$

Then for each pair of indices  $i, j \in \{1, \dots, n\}$  we obtain the  $2 \times 2$  system

$$(3.16) \quad \begin{bmatrix} 1 + \frac{\beta \Delta t}{2} & \frac{\Delta t}{2} \left( \alpha - \frac{1}{h^2 \kappa^2} (\lambda_i + \lambda_j) \right) \\ -\frac{\Delta t}{2} \left( \alpha - \frac{1}{h^2 \kappa^2} (\lambda_i + \lambda_j) \right) & 1 + \frac{\beta \Delta t}{2} \end{bmatrix} \begin{bmatrix} \hat{V}_{ij} \\ \hat{W}_{ij} \end{bmatrix} = \begin{bmatrix} \hat{V}_{ij}^n \\ \hat{W}_{ij}^n \end{bmatrix}.$$

Defining

$$(3.17) \quad c = 1 + \frac{\beta \Delta t}{2}, \quad d = \frac{\Delta t}{2} \left( \alpha - \frac{1}{h^2 \kappa^2} (\lambda_i + \lambda_j) \right),$$

we may rewrite (3.16) as

$$(3.18) \quad \begin{bmatrix} c & d \\ -d & c \end{bmatrix} \begin{bmatrix} \hat{V}_{ij} \\ \hat{W}_{ij} \end{bmatrix} = \begin{bmatrix} \hat{V}_{ij}^n \\ \hat{W}_{ij}^n \end{bmatrix},$$

which by Cramer's rule gives the midpoint values

$$(3.19) \quad \hat{V}_{ij} = \frac{c \hat{V}_{ij}^n - d \hat{W}_{ij}^n}{c^2 + d^2}, \quad \hat{W}_{ij} = \frac{d \hat{V}_{ij}^n + c \hat{W}_{ij}^n}{c^2 + d^2}.$$

By linearity of the discrete sine transform,  $\hat{V}$  and  $\hat{W}$  are averages of  $\hat{V}^{n+1}$  and  $\hat{V}^n$  and of  $\hat{W}^{n+1}$  and  $\hat{W}^n$ , that is  $\hat{V}_{ij}^{n+1} = 2\hat{V}_{ij} - \hat{V}_{ij}^n$  (and similarly for  $\hat{W}$ ). Since we are interested in computing  $\hat{V}^{n+1}$  and  $\hat{W}^{n+1}$  we now express the full system in terms of non-averaged quantities

$$(3.20) \quad \begin{bmatrix} c & d \\ -d & c \end{bmatrix} \begin{bmatrix} \hat{V}_{ij}^{n+1} \\ \hat{W}_{ij}^{n+1} \end{bmatrix} = \begin{bmatrix} 2-c & -d \\ d & 2-c \end{bmatrix} \begin{bmatrix} \hat{V}_{ij}^n \\ \hat{W}_{ij}^n \end{bmatrix}.$$

Inverting the left-hand side, the direct update rule is

$$(3.21) \quad \begin{bmatrix} \hat{V}_{ij}^{n+1} \\ \hat{W}_{ij}^{n+1} \end{bmatrix} = \frac{1}{c^2 + d^2} \begin{bmatrix} c(2-c) - d^2 & -2d \\ 2d & c(2-c) - d^2 \end{bmatrix} \begin{bmatrix} \hat{V}_{ij}^n \\ \hat{W}_{ij}^n \end{bmatrix}.$$

The update matrix in (3.21) has the form  $\frac{1}{c^2+d^2}(pI + qJ)$  where  $J = \begin{bmatrix} 0 & -1 \\ 1 & 0 \end{bmatrix}$  and

$$(3.22) \quad p = c(2-c) - d^2, \quad q = 2d.$$

Since any matrix of the form  $pI + qJ$  can be decomposed as  $\sqrt{p^2 + q^2} \begin{bmatrix} \cos \theta & -\sin \theta \\ \sin \theta & \cos \theta \end{bmatrix}$ , we can write

$$(3.23) \quad \begin{bmatrix} \hat{V}_{ij}^{n+1} \\ \hat{W}_{ij}^{n+1} \end{bmatrix} = \phi \begin{bmatrix} \cos \theta & -\sin \theta \\ \sin \theta & \cos \theta \end{bmatrix} \begin{bmatrix} \hat{V}_{ij}^n \\ \hat{W}_{ij}^n \end{bmatrix}$$

where

$$(3.24) \quad \theta = \arctan\left(\frac{q}{p}\right) = \arctan\left(\frac{2d}{c(2-c) - d^2}\right), \quad \phi = \frac{\sqrt{p^2 + q^2}}{c^2 + d^2}.$$

The prefactor  $\phi$  controls the amplitude change at each step. When  $\beta = 0$  we have  $c = 1$ , so  $p = 1 - d^2$ ,  $q = 2d$ , and  $p^2 + q^2 = (1 + d^2)^2 = (c^2 + d^2)^2$ , giving  $\phi = 1$ . In this case the scheme reduces to a pure rotation

$$(3.25) \quad \begin{bmatrix} \hat{V}_{ij}^{n+1} \\ \hat{W}_{ij}^{n+1} \end{bmatrix} = \begin{bmatrix} \cos \theta & -\sin \theta \\ \sin \theta & \cos \theta \end{bmatrix} \begin{bmatrix} \hat{V}_{ij}^n \\ \hat{W}_{ij}^n \end{bmatrix}$$

with  $\theta = 2\arctan(d)$ , and the scheme is norm-preserving. When  $\beta \neq 0$ , we have  $\phi < 1$ , and the update introduces damping at each step, consistent with the dissipative terms  $-\beta V$ ,  $-\beta W$  in (3.3). Once  $\hat{V}^{n+1}$  and  $\hat{W}^{n+1}$  have been computed in the transformed basis via (3.23), the solution in the original variables is recovered by inverting the transform in (3.14),

$$(3.26) \quad V^{n+1} = Z\hat{V}^{n+1}Z^T, \quad W^{n+1} = Z\hat{W}^{n+1}Z^T,$$

which, like the forward transform, can be applied in  $O(n^2 \log n)$  operations via the discrete sine transform.

**4. Low-rank implementation of the OFT.** In this section we first review the basic low rank arithmetic used in the low-rank OFT solver.

**4.1. Low-rank arithmetic: rounded sum of matrices.** During each step of a Schrödinger solve we must compute sums of low-rank matrices. Since the sum of low-rank matrices in general is not low-rank, we must re-truncate the sum after it is computed. We have several summands  $C_i$  in their SVD form,  $U_i, \Sigma_i, V_i^T$  and we want to compute

$$(4.1) \quad X = U_X \Sigma_X V_X^T = \sum_{j=1}^s C_j = \sum_{j=1}^s U_j \Sigma_j V_j^T.$$

We recognize that we can write this sum as

$$(4.2) \quad \sum_{j=1}^s U_j \Sigma_j V_j^T = [U_1 \quad \cdots \quad U_s] \begin{bmatrix} \Sigma_1 & & \\ & \ddots & \\ & & \Sigma_s \end{bmatrix} \begin{bmatrix} V_1^T \\ \vdots \\ V_s^T \end{bmatrix} = U_{big} \Sigma_{big} V_{big}^T$$

but in general neither  $U_{big}$  or  $V_{big}^T$  will have orthogonal columns, so  $U_{big} \Sigma_{big} V_{big}^T$  is not a valid SVD of  $X$ . To obtain an orthogonal basis for  $U_{big}$  and  $V_{big}$  we perform column pivoted QR decompositions

$$(4.3) \quad U_{big} = Q_U R_U \Pi_U^T, \quad V_{big} = Q_V R_V \Pi_V^T$$

and form

$$(4.4) \quad L = R_U \Pi_U^T \Sigma_{big} \Pi_V R_V^T,$$

which then allows us to write  $X$  as

$$(4.5) \quad X = Q_U L Q_V^T.$$

Since we want to return  $X$  in its SVD form  $X = U_X \Sigma_X V_X^T$ , we can take the SVD of  $L$  and write

$$(4.6) \quad U_X \Sigma_X V_X^T = (Q_U U_L) \Sigma_L (V_L^T Q_V^T)$$

after we truncate  $U_L \Sigma_L V_L^T$  by the singular values in  $\Sigma_L$  to some proscribed tolerance. The full algorithm is described in [Algorithm 4.1](#).

**4.2. Cross-DEIM.** In this section we describe how to find a low-rank SVD approximation of some matrix  $G \in \mathbb{R}^{m \times n}$  via the Cross-DEIM algorithm introduced in [1]. This algorithm scales sub-linearly with the number of elements, which is an improvement over the traditional truncated SVD, as it is a sampling method and does not require construction of the full matrix  $G$ . Cross-DEIM is based on an iterative combination of cross-approximation and index selection.

---

**Algorithm 4.1** Rounding of sum of low-rank matrices,  $U_X \Sigma_X V_X^T = \mathcal{T}_{\epsilon, r_{\max}}^{\text{round}}(\sum_{j=1}^s U_j \Sigma_j V_j^T)$

---

**Input:** Low-rank matrices in the form  $U_j \Sigma_j V_j^T, j = 1, \dots, s$ , tolerance  $\epsilon$ , max rank  $r_{\max}$

**Output:**  $U_X, \Sigma_X, V_X^T$

Let  $U = [U_1, \dots, U_s], \Sigma = \text{diag}(\Sigma_1, \dots, \Sigma_s), V = [V_1, \dots, V_s]$

Perform column pivoted QR:  $[Q_U, R_U, \Pi_U] = \text{qr}(U), [Q_V, R_V, \Pi_V] = \text{qr}(V)$

Compute the truncated SVD for the small matrix with tolerance  $\epsilon$  and max rank  $r_{\max}$ :

$$\mathcal{T}_{\epsilon, r_{\max}}(R_U \Pi_U \Sigma \Pi_V^T R_V^T) = U \Sigma V^T$$

Form  $U_X \leftarrow Q_1 U, V_X \leftarrow Q_2 V$

**return**  $[U_X, \Sigma_X, V_X]$

---

Given our low-rank matrix  $G$ , cross-approximation attempts to find a matrix  $M \in \mathbb{R}^{r_1 \times r_2}$  such that

$$(4.7) \quad G \approx G(:, \mathcal{J}) M G(\mathcal{I}, :),$$

where  $\mathcal{I}$  and  $\mathcal{J}$  are two index sets selecting  $r_2$  rows and  $r_1$  columns, respectively. We choose  $M = G(\mathcal{I}, \mathcal{J})^+$  where the pseudo-inverse can stably computed using methods from [7, 1].

Given a function handle to  $G(i, j)$  and the two index sets  $\mathcal{I}$  and  $\mathcal{J}$ , the subroutine `scross`, as detailed in Algorithm 4.3, returns a singular value decomposition  $U S V^T = G(:, \mathcal{J}) M G(\mathcal{I}, :) \approx G$ .

The quality of the approximation rely on the appropriate selection of  $\mathcal{I}$  and  $\mathcal{J}$ . Optimally solving the index selection problem requires knowledge of the full matrix  $G$  which defeats the purpose of our cross-approximation. Instead, given the singular vectors  $U$  and  $V$ , we follow a greedy procedure for selecting  $\mathcal{I}$  and  $\mathcal{J}$ . Among potential options are DEIM [15], QDEIM [8], and leverage scores [13]. Here we exclusively use QDEIM as described in Algorithm 4.2.

We can resolve the index selection dilemma, i.e. that we don't want to form the whole matrix  $G$ , but optimally selecting  $\mathcal{I}$  and  $\mathcal{J}$  requires the full  $G$ , by iteration which is the direction employed in Cross-DEIM.

---

**Algorithm 4.2**  $[\mathcal{I}] = \text{QDEIM}(U)$

QDEIM index selection

---

1: **Input:** Orthogonal matrix  $U$  of size  $k \times l$

2: **Output:** Index set  $\mathcal{I}$  of size  $l$

3:  $[\sim, \sim, p] = \text{qr}(U^T, \text{'vector'})$  {Perform column pivoted QR on  $U^T$ .}

4:  $\mathcal{I} = P(1 : l)$

5: **return**  $\mathcal{I}$ .

---

We note that the cross approximation is distinct from the CUR approximation that computes  $M$  by projection  $M = G(:, \mathcal{J})^+ G G(\mathcal{I}, :)^+$ . The CUR approximation requires access to the entire matrix  $G$  it cannot be computed with sub-linear cost in space.

Cross-DEIM begins by initializing two empty index sets, one for the rows and one for the columns. At each iteration  $k$  the index sets are updated with the indices selected by QDEIM, and stabilized cross approximation is performed. Linearly dependent rows and columns are

removed as needed. This is repeated until convergence or the maximum number of iterations are reached. The main computational cost comes from the cross-approximation and scales as  $O((m+n)r^2)$ . We assume the iteration number remains  $O(1)$ , which gives a sublinear cost overall. The full algorithm is outlined in [Algorithm A.1](#).

---

**Algorithm 4.3** [U,S,V,rC,rR] = `scross(G,I,J)`

Stabilized cross approximation of  $G$

- 
- 1: **Input:**  $G$ , and two index sets  $\mathcal{I}, \mathcal{J}$  with  $k$  and  $l$  elements, respectively.
  - 2: **Output:** Approximate SVD of  $G$ ,  $U \in \mathbb{R}^{m \times r}$ ,  $S \in \mathbb{R}^{r \times r}$ ,  $V \in \mathbb{R}^{r \times n}$ , and two vectors to test for linear dependence  $r_R, r_C \in \mathbb{R}^r$ .
  - 3:  $C = G(:, \mathcal{J}) \in \mathbb{R}^{m \times k}$ ,  $R = G(\mathcal{I}, :) \in \mathbb{R}^{l \times n}$
  - 4:  $CP_C = QR_C$ ,  $R^T P_R = ZR_R$  {Perform column pivoted QR.}
  - 5: **if**  $k \leq l$  **then**
  - 6:   Solve  $Q(\mathcal{I}, :)W = R$  {Solved using \ if  $Q(\mathcal{I}, :)$  is well conditioned,}
  - 7:   {else solved by truncated SVD pseudoinverse.}
  - 8:    $W = \hat{U}SV^T$  {Perform truncated SVD.}
  - 9:    $U = Q\hat{U}$
  - 10: **else**
  - 11:   Solve  $Z(:, \mathcal{J})W = C^T$  {Solved using \ if  $Z(:, \mathcal{J})$  is well conditioned,}
  - 12:   {else solved by truncated SVD pseudoinverse.}
  - 13:    $W^T = US\hat{V}^T$  {Perform truncated SVD.}
  - 14:    $V = Z\hat{V}$
  - 15: **end if**
  - 16: **return**  $USV^T \approx G$  and  $r_R = \text{diag}(P_R^T R_R P_R)$ ,  $r_C = \text{diag}(P_C^T R_C P_C)$ .
- 

---

**Algorithm 4.4** `v = Helmholtz-OFT(g, alpha, beta, kappa, Delta_t0, Delta_tf, T, epsilon)`

Low-rank OFT Helmholtz solve:  $v = A^{-1}g$  via  $v = f(A)^2g$ , where  $A = m(\mathbf{x}) + \Delta/\kappa^2$  and  $f(A) = A^{-1/2}$

- 
- 1: **Input:** Source term  $g \in \mathbb{C}^{n \times n}$ , parameters  $\alpha, \beta, \kappa$ , initial step size  $\Delta t_0$ , final step size  $\Delta t_f$ , final time  $T$ , tolerance  $\epsilon$
  - 2: **Output:** Approximate solution  $v \approx A^{-1}g$  in low-rank form  $U_V \Sigma_V V_V^T + i U_W \Sigma_W V_W^T$
  - 3: Compute exponential time grid  $\{\tau_n\}$  via (2.12)
  - 4: Compute Fresnel quadrature weights  $\{\omega_n\}$  via (2.15)
  - 5:  $[U_W, \Sigma_W, V_W], [U_V, \Sigma_V, V_V] \leftarrow \text{OFT-SqrtInv}(W^{(0)\text{-factors}}, V^{(0)\text{-factors}}, \{\tau_k\}, \{\omega_k\}, \alpha, \beta, \kappa, \epsilon)$   
{Pass 1:  $v_1 = A^{-1/2}g$ .}
  - 6:  $[U_W, \Sigma_W, V_W], [U_V, \Sigma_V, V_V] \leftarrow \text{OFT-SqrtInv}([U_W, \Sigma_W, V_W], [U_V, \Sigma_V, V_V], \{\tau_k\}, \{\omega_k\}, \alpha, \beta, \kappa, \epsilon)$   
{Pass 2:  $v = A^{-1/2}v_1 = A^{-1}g$ .}
  - 7:  $v \leftarrow U_V \Sigma_V V_V^T + i U_W \Sigma_W V_W^T$  {Reconstruct complex solution.}
  - 8: **return**  $v$
- 

**4.3. The low-rank OFT solver.** Throughout this method, both  $V$  and  $W$  are stored as low-rank SVDs and the full matrices are never formed. Each time step transforms the factor matrices via the DST, applies the rotation in (3.23), and transforms back. Because the DST

is linear, it acts on the factor matrices directly: applying it to the columns of  $U_V$  and  $V_V$  (and similarly for  $W$ ) yields the factors of  $\hat{V}^n$  and  $\hat{W}^n$  without ever assembling the dense matrix.

The rotation itself acts element-wise, so we use the Cross-DEIM algorithm to construct a low-rank factorization of  $\hat{V}^{n+1}$  and  $\hat{W}^{n+1}$  by sampling individual entries as in (3.23). Each entry depends only on  $\hat{V}_{ij}^n$ ,  $\hat{W}_{ij}^n$ , and the scalars  $\theta_{ij}$  and  $\phi_{ij}$ . Each entry evaluation then reduces to two inner products keeping the per-entry cost low.

At each time step the current result is accumulated with `truncsum`. This algorithm performs a low rank sum of several matrices in their SVD form, concatenated into a cell structure, and is further described in subsection 4.1. The full algorithm for solving the Helmholtz equation via two applications of the inverse square root Helmholtz operator is given in Algorithm 4.4. Here the operator is the Helmholtz operator  $A = m(\mathbf{x}) + \Delta/\kappa^2$  introduced in section 2, so that the discrete solution to (1.1) is  $v = A^{-1}g = f(A)^2g$  with  $f(A) = A^{-1/2}$ . The algorithm calls Algorithm A.2 to evaluate each OFT integral and Algorithm 4.5 to advance the Schrödinger equation by one step.

**4.4. Low-rank timestepping of the Schrödinger equation.** We will now describe the low-rank implementation of the method described in subsection 3.1. We begin with the factors  $V$  and  $W$  in low-rank form from the previous time step. In line 3 the discrete sine transform is applied as in (3.14). Lines 5 through 10 define, but do not evaluate, the two entry wise functions that are passed as function handles to Cross-DEIM to evaluate only for selected indices. Lines 11 and 12 call Cross-DEIM to evaluate (3.23) only for the indices that it selects. On lines 13 and 14 we reapply the discrete sine transform to the singular vectors of  $V$  and  $W$ , and return.

**5. Experimental results.** Here we will discuss the results of numerical experiments using our method, and compare them to the results obtained when not using low-rank approximation. All results were obtained on an Apple Macbook Air M3 with 16 GB of memory, running MacOS 26.3.1 (a). For both problems we take the Cross-DEIM error tolerance to be  $\Delta t^3$ , while the `truncsum` error tolerance is set to  $10^{-12}$ . In all cases the maximum allowed rank is taken to be the full size of the mesh in either dimension.

**5.1. Example 1.** For our first experiment we solve the differential equation

$$(5.1) \quad \begin{aligned} u(\mathbf{x}) - i\Delta u(\mathbf{x}) &= f(\mathbf{x}), & \mathbf{x} \in \Omega, \\ u(\mathbf{x}) &= 0, & \mathbf{x} \in \partial\Omega, \end{aligned}$$

on the domain  $\Omega = [0, 1]^2$ , where  $\mathbf{x} = (x, y)$  and the right-hand side is

$$(5.2) \quad f(\mathbf{x}) = (1 + i\pi^2(k^2 + l^2)) \sin(k\pi x) \sin(l\pi y).$$

This corresponds to the simplified case of the framework described in section 3 with  $\alpha = \beta = 0$  and  $\kappa = 1$ , so that  $m(\mathbf{x}) \equiv 1$ . In this case we take our operator to be  $A = \Delta$ , so that (5.1) can be written as  $(I - i\Delta)u = f$ . We choose this as our first example because there is a closed form solution to compare to that is known to be low-rank. One may verify that the solution to (5.1) is

$$(5.3) \quad u(\mathbf{x}) = \sin(k\pi x) \sin(l\pi y).$$

**Algorithm 4.5** [W-factors, V-factors] = LR-Timestep(W-factors, V-factors,  $\{\lambda_j\}$ ,  $\Delta t$ ,  $\alpha$ ,  $\beta$ ,  $\kappa$ )

Low-rank time step for the Schrödinger equation via rotation in eigenspace

- 1: **Input:** Low-rank factors  $U_W \Sigma_W V_W^T, U_V \Sigma_V V_V^T$ ; eigenvalues  $\{\lambda_j\}$ ; step size  $\Delta t$ ; parameters  $\alpha, \beta, \kappa$
- 2: **Output:** Updated low-rank factors for  $W$  and  $V$
- 3:  $\hat{U}_W \leftarrow \text{DST}(U_W)$ ,  $\hat{V}_W \leftarrow \text{DST}(V_W)$ ,  $\hat{U}_V \leftarrow \text{DST}(U_V)$ ,  $\hat{V}_V \leftarrow \text{DST}(V_V)$  {Transform factors via DST.}
- 4: Define entry-wise functions  $f_W(i, j)$  and  $f_V(i, j)$ :
- 5:  $w \leftarrow (\hat{U}_W(i, :) \Sigma_W) \cdot \hat{V}_W(j, :)^T$
- 6:  $v \leftarrow (\hat{U}_V(i, :) \Sigma_V) \cdot \hat{V}_V(j, :)^T$
- 7:  $c \leftarrow 1 + \beta \Delta t / 2$ ,  $d \leftarrow \frac{\Delta t}{2} \left( \alpha - \frac{\lambda_i + \lambda_j}{\kappa^2} \right)$
- 8:  $p \leftarrow c(2 - c) - d^2$ ,  $q \leftarrow 2d$ ,  $\theta \leftarrow \arctan(q, p)$ ,  $\phi \leftarrow \sqrt{p^2 + q^2} / (c^2 + d^2)$
- 9:  $f_W(i, j) \leftarrow \phi(\sin \theta v + \cos \theta w)$
- 10:  $f_V(i, j) \leftarrow \phi(\cos \theta v - \sin \theta w)$
- 11:  $[\hat{U}_W, \Sigma_W, \hat{V}_W] \leftarrow \text{Cross-DEIM}(f_W, \hat{U}_W, \hat{V}_W, \Delta t^3, n)$
- 12:  $[\hat{U}_V, \Sigma_V, \hat{V}_V] \leftarrow \text{Cross-DEIM}(f_V, \hat{U}_V, \hat{V}_V, \Delta t^3, n)$
- 13:  $U_W \leftarrow \text{DST}(\hat{U}_W)$ ,  $V_W \leftarrow \text{DST}(\hat{V}_W)$  {Transform back via DST.}
- 14:  $U_V \leftarrow \text{DST}(\hat{U}_V)$ ,  $V_V \leftarrow \text{DST}(\hat{V}_V)$
- 15: **return**  $[U_W, \Sigma_W, V_W], [U_V, \Sigma_V, V_V]$

With the OFT, we can write the solution as

$$(5.4) \quad u(\mathbf{x}) = \int_0^\infty e^{-\tau} e^{i\tau\Delta} f(\mathbf{x}) d\tau.$$

We then define

$$(5.5) \quad \hat{u}(\mathbf{x}, \tau) = e^{i\tau\Delta} f(\mathbf{x}),$$

which is the solution to the initial value problem

$$(5.6) \quad \begin{aligned} \hat{u}_\tau &= i\Delta \hat{u}, & \mathbf{x} \in \Omega, \\ \hat{u}(\mathbf{x}, 0) &= f(\mathbf{x}), & \mathbf{x} \in \Omega. \end{aligned}$$

The IVP (5.6) is evaluated using the low-rank scheme discussed in [section 3](#). In this case we will make use of a simpler quadrature for the OFT integral. Instead of the exponential scheme described in [subsection 2.3](#), we instead approximate the integral with the trapezoidal rule over the pseudo-time domain  $[0, T_f]$ , giving

$$(5.7) \quad u(\mathbf{x}) \approx \sum_{j=0}^{N-1} \frac{\tau_{j+1} - \tau_j}{2} (e^{-\tau_j} \hat{u}(\mathbf{x}, \tau_j) + e^{-\tau_{j+1}} \hat{u}(\mathbf{x}, \tau_{j+1})).$$

In our computation we simplify this by writing the sum as

$$(5.8) \quad u(\mathbf{x}) \approx \sum_{j=0}^{N-1} w_j \hat{u}(\mathbf{x}, \tau_j),$$

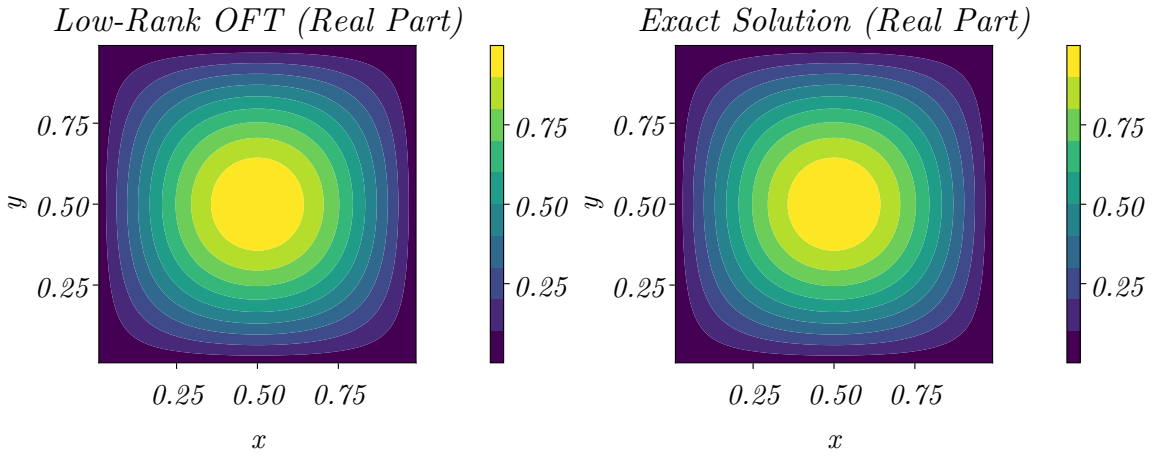


**Figure 1.** Computed low rank solution to (5.1) compared with the exact solution (5.3), with  $T = 100$ ,  $\Delta t = 0.01$ , and  $n = 100$ .

where the weights  $w_j$  are precomputed as

$$(5.9) \quad \begin{aligned} w_0 &= \frac{\tau_1 - \tau_0}{2} e^{-\tau_0}, \\ w_j &= \frac{\tau_{j+1} - \tau_{j-1}}{2} e^{-\tau_j}, \quad 0 < j < N - 1, \\ w_{N-1} &= \frac{\tau_{N-1} - \tau_{N-2}}{2} e^{-\tau_{N-1}}. \end{aligned}$$

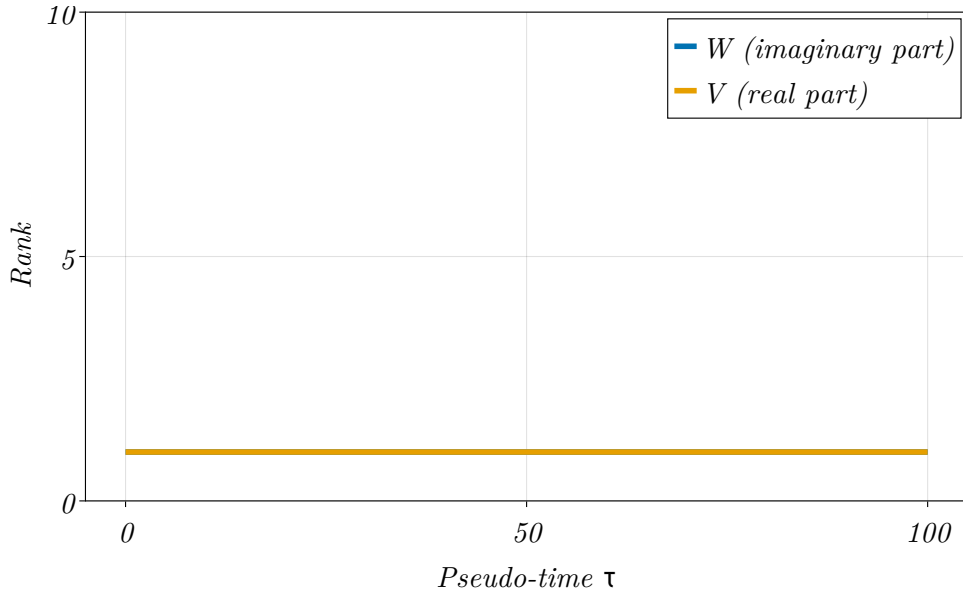


**Figure 2.** Rank of the computed solution matrix over time.

We see that the rank remains one over all time steps. This is due to the fact that the exact solution  $u$  is a superposition of a few eigenfunctions of the operator. The solution simply scales the initial condition over time without introducing new modes to the system.

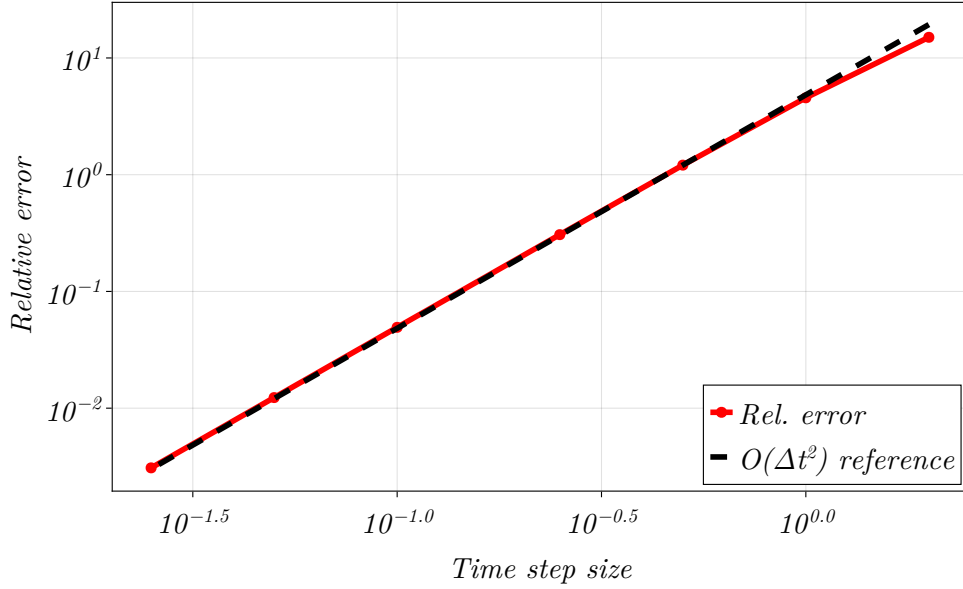


**Figure 3.** Scaling of the computed solution’s error with respect to different time step sizes, with  $T = 100$  and  $n = 100$ .

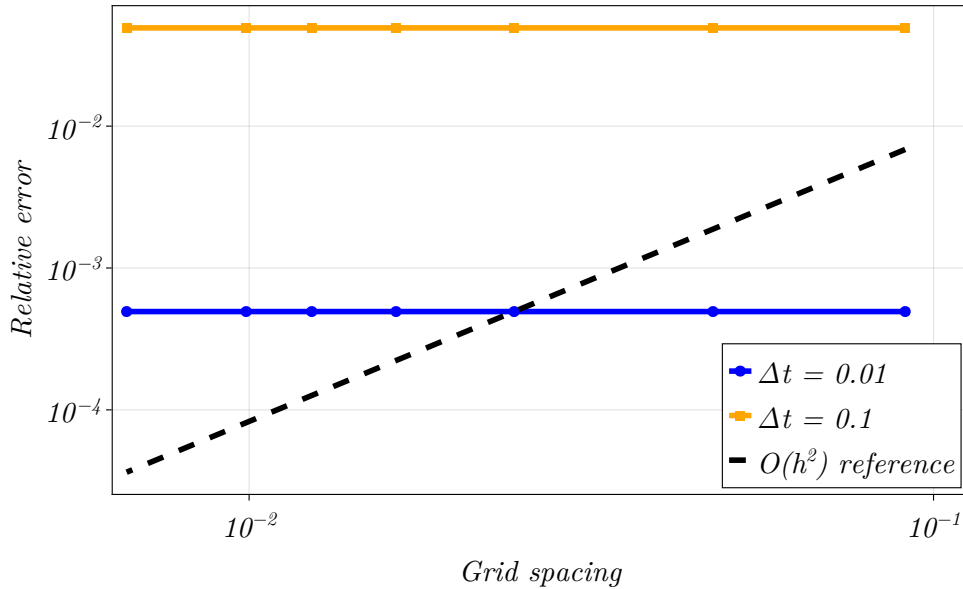


**Figure 4.** Scaling of the computed solution’s error with respect to different levels of mesh refinement. We note that the relative error for  $\Delta t = 0.1$  remains a constant  $4.926 \times 10^{-2}$  while the error for  $\Delta t = 0.01$  remains  $4.931 \times 10^{-4}$ , which again demonstrates second order accuracy in time.

Here we see that the error scales with  $\Delta t^2$ , while the spatial error remains constant. Again this is expected behavior, as the solution is a superposition of eigenfunctions and is rank 1, we do not expect to decrease our error by increasing our spatial resolution.

**5.2. Example 2.** We will now solve the Helmholtz problem described in section [section 3](#), i.e.

$$(5.10) \quad \begin{aligned} X_t &= i \left( (m(\mathbf{x}) - 1) X + \frac{\Delta}{\kappa^2} X \right), & \mathbf{x} \in \Omega, \\ X(\mathbf{x}, t) &= 0, & \mathbf{x} \in \partial\Omega, \\ X(\mathbf{x}, 0) &= g(\mathbf{x}), & \mathbf{x} \in \Omega, \end{aligned}$$

on the domain  $\Omega = [-\pi, \pi]^2$ , where  $\mathbf{x} = (x, y)$ . For these experiments we take  $g(\mathbf{x}) = \exp(-6(x^2 + y^2))$ ,  $\kappa = 2$ , and constant coefficients  $\alpha = 2$  and  $\beta = 0.1$ , so that  $m(\mathbf{x}) - 1 = 2 + 0.1i$  throughout  $\Omega$ . Note that  $g(\mathbf{x})$  does not vanish on  $\partial\Omega$ , but we take it to be zero as an approximation. We expect the total error to take the form  $\epsilon = ch^2 + d\Delta t^2 + p\exp(-\gamma T)$ , and by regressing over sets of the step size  $h$ , the time step  $\Delta t$ , and the final time  $T$  we find that  $c \approx 10^1$ ,  $d \approx 10^0$ ,  $p \approx 10^0$ , and  $\gamma \approx 10^{-1}$ . We therefore take  $T = 100$  to minimize the error due to the truncation of the OFT integral, which is over  $[0, \infty)$ , to  $T$ .

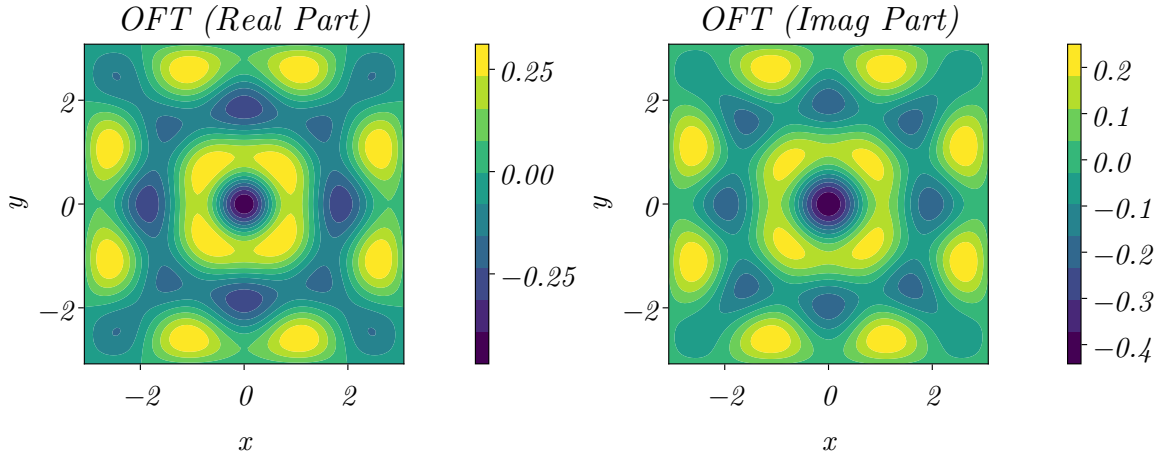


**Figure 5.** Computed low rank solution to (5.10) with  $T = 20$ ,  $\Delta t_0 = 0.01$ , and  $n = 100$ . Note that the scale is slightly different for the real and the imaginary parts.

We see in this example that for this choice of  $g$  the rank does vary with time. The rank of the  $V$  and  $W$  matrices never reaches higher than 15, much less than their size when reconstructed from the SVD form, which in this case is 100 by 100. We also note that the rank history follows the same pattern, a sharp rise and an asymptotic settling, for both OFT passes, but for the second pass the rank remains slightly smaller than for the first pass throughout.

In juxtaposition with the first example, we see that the error with respect to  $\Delta t$  quickly saturates even for a higher resolution mesh ( $n = 200$ ), and we do observe second order accuracy with respect to the mesh refinement. When we instead jointly vary  $\Delta t$  and  $h$ , we see that the error decreases as approximately  $h^2 + \Delta t^2$ .

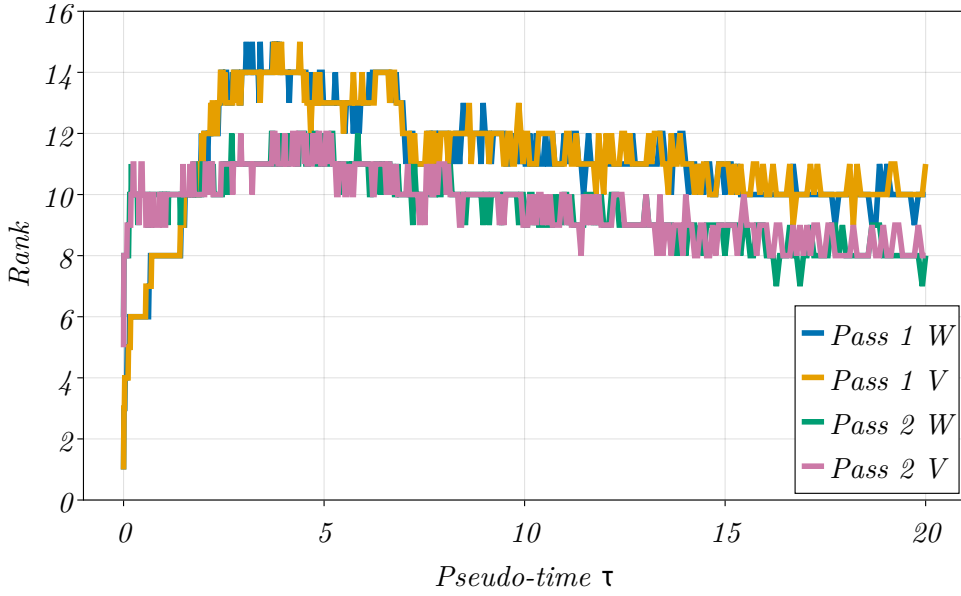


**Figure 6.** Rank of the computed solution matrix over time for a grid with 100 points in each dimension.

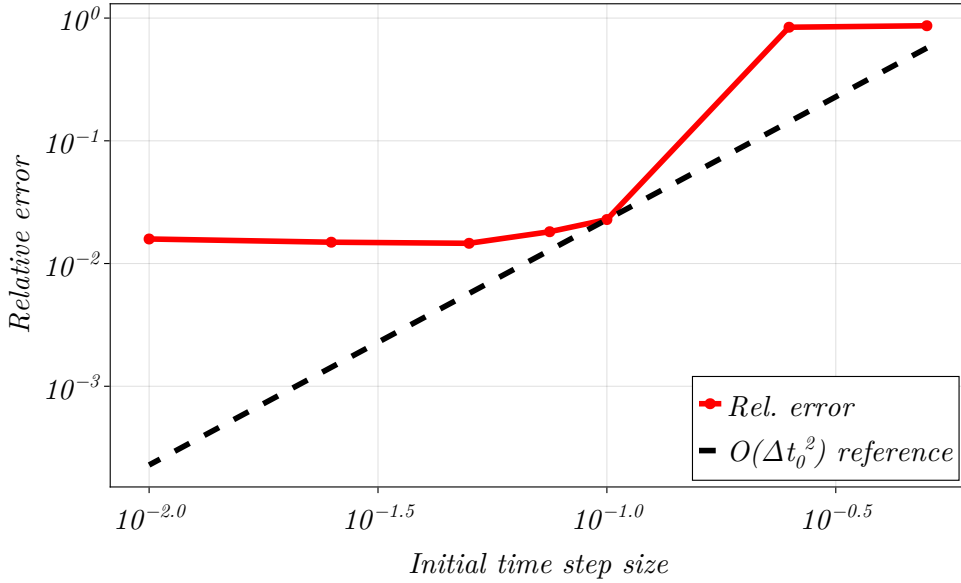


**Figure 7.** Scaling of the computed solution's error with respect to different time step sizes with  $T = 100$  and  $n = 200$ .

**6. Conclusions.** Through our experiments we see that the OFT framework lends itself well to the usage of low-rank methods. Our results show that our solver is able to obtain a result with small error, and for certain source terms the computational cost becomes much lower than it would be using a traditional solver.

The second order accuracy we observe in [Figure 9](#) is expected, as our low rank method is

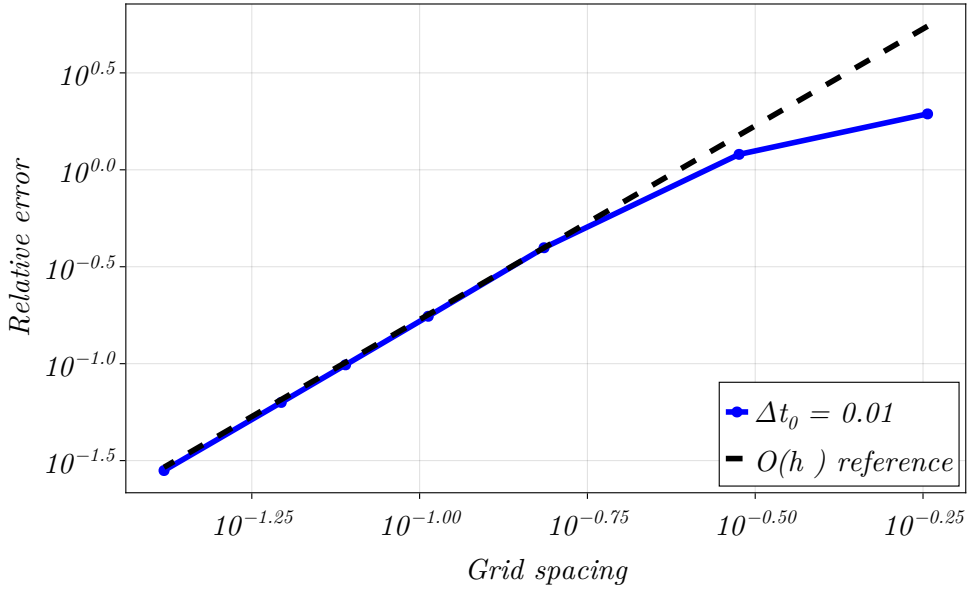


**Figure 8.** Scaling of the computed solution’s error with respect to different levels of mesh refinement with  $T = 100$ .

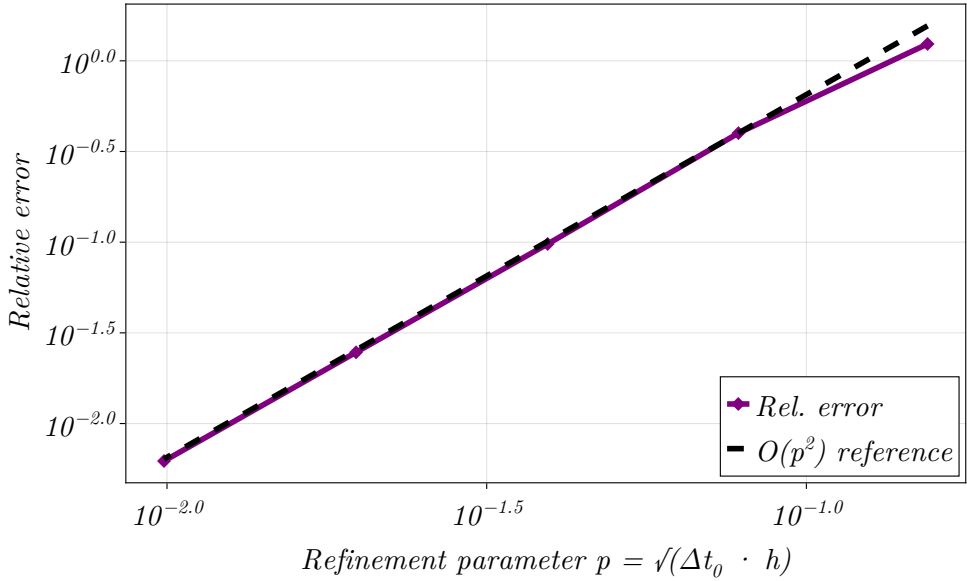


**Figure 9.** Scaling of the computed solution’s error while jointly varying  $\Delta t$  and  $h$  with  $T = 100$ .

essentially a trapezoidal rule, seen clearly in (3.11) where the right hand side is evaluated at an average value instead of at one endpoint.

**Acknowledgments.** Research is supported by Virginia Tech.

**Appendix A. Appendix.**

---

**Algorithm A.1**  $[U, S, V] = \text{Cross-DEIM}(G, U_0, V_0, \epsilon, r_{\max}, \aleph_{\max}, \text{maxiter})$ 


---

 Adaptive Cross-DEIM approximation to  $G \in \mathbb{R}^{m \times n}$ 


---

- 1: **Input:** Matrix  $G \in \mathbb{R}^{m \times n}$ , initial rank  $r$  guess to the singular vector matrix  $U_0 \in \mathbb{R}^{m \times r}$ ,  $V_0 \in \mathbb{R}^{n \times r}$ , tolerance  $\epsilon$ , maximum output rank  $r_{\max}$ , maximum index set cardinality  $\aleph_{\max}$ , maximum number of iterations **maxiter**.
  - 2: **Output:** Approximate SVD of  $G$ ,  $U \in \mathbb{R}^{m \times r}$ ,  $S \in \mathbb{R}^{r \times r}$ ,  $V \in \mathbb{R}^{r \times n}$ .
  - 3: Set  $\mathcal{I}_0 = \mathcal{J}_0 = \emptyset$ .
  - 4: **for**  $k = 1, 2, \dots, \text{maxiter}$  **do**
  - 5:    $\mathcal{I}_k^* = \text{QDEIM}(U_{k-1})$
  - 6:    $\mathcal{J}_k^* = \text{QDEIM}(V_{k-1})$  { QDEIM can be replaced by DEIM }
  - 7:    $\mathcal{I}_k = \mathcal{I}_k^* \cup \mathcal{I}_{k-1}$ ,  $\mathcal{J}_k \leftarrow \mathcal{J}_k^* \cup \mathcal{J}_{k-1}$  {Note that the index sets are ordered by QDEIM.}
  - 8:   **if**  $|\mathcal{I}_k| = |\mathcal{I}_{k-1}|$  or  $k = 1$  **then** {Make sure that the index set increase by one}
  - 9:      $\mathcal{I}_k = \mathcal{I}_k^* \cup \{i_{\text{rand}} \in \mathbb{C}(\mathcal{I}_k^*)\}$  {using a random  $i_{\text{rand}}$  from the complement of  $\mathcal{I}_k^*$ .}
  - 10:   **end if**
  - 11:   **if**  $|\mathcal{J}_k| = |\mathcal{J}_{k-1}|$  or  $k = 1$  **then**
  - 12:      $\mathcal{J}_k \leftarrow \mathcal{J}_k^* \cup \{j_{\text{rand}} \in \mathbb{C}(\mathcal{J}_k^*)\}$
  - 13:   **end if**
  - 14:   **if**  $|\mathcal{I}_k| > \aleph_{\max}$  **then**
  - 15:      $\mathcal{I}_k \leftarrow \mathcal{I}_k(1 : \aleph_{\max})$  {Keep the  $\aleph_{\max}$  most important indices.}
  - 16:   **end if**
  - 17:   **if**  $|\mathcal{J}_k| > \aleph_{\max}$  **then**
  - 18:      $\mathcal{J}_k \leftarrow \mathcal{J}_k(1 : \aleph_{\max})$
  - 19:   **end if**
  - 20:    $[U_k, S_k, V_k, r_C, r_R] = \text{scross}(G, \mathcal{I}_k, \mathcal{J}_k)$
  - 21:   **for**  $l = 1, 2, \dots, |\mathcal{I}_k|$  **do**
  - 22:     **if**  $|(r_R)_l| < 10^{-12}$  **then**
  - 23:       Remove element  $l$  from  $\mathcal{I}_k$  {Remove redundant rows in  $R = G(\mathcal{I}_k, :)$ .}
  - 24:     **end if**
  - 25:   **end for**
  - 26:   **for**  $l = 1, 2, \dots, |\mathcal{I}_k|$  **do**
  - 27:     **if**  $|(r_C)_l| < 10^{-12}$  **then**
  - 28:       Remove element  $l$  from  $\mathcal{J}_k$  {Remove redundant columns in  $C = G(:, \mathcal{J}_k)$ .}
  - 29:     **end if**
  - 30:   **end for**
  - 31:    $\phi = \|U_k S_k V_k^T - U_{k-1} S_{k-1} V_{k-1}^T\|$ ,  $S_{\min} = \min(\text{diag}(S_k))$
  - 32:    $\eta_1 = \|(I(:, \mathcal{I}_k))^T U_k\|_2^{-1}$ ,  $\eta_2 = \|V_k^T I(\mathcal{J}_k, :)\|_2^{-1}$
  - 33:   **if**  $\max(\phi, \min(\eta_1(1 + \eta_2), \eta_2(1 + \eta_1)) S_{\min}) < \epsilon$  **then**
  - 34:     Break out of for loop {Above  $S_{\min}$  is the smallest s.v. in the  $k$ th approx.}
  - 35:   **end if**
  - 36: **end for**
  - 37: Find  $r^*$  so that  $\sum_{l=r^*+1}^{\min(m,n)} S_l^2 < \epsilon^2$
  - 38: Set  $r = \max(\min(r^*, r_{\max}), 1)$
  - 39: **return**  $U_k(:, 1 : r)$ ,  $S_k(1 : r, 1 : r)$ ,  $V_k(:, 1 : r)$
-

The full Helmholtz solver is given in [Algorithm 4.4](#). It calls [Algorithm A.2](#) twice to evaluate  $f(A) = A^{-1/2}$ , which in turn calls [Algorithm 4.5](#) at each quadrature node to advance the Schrödinger equation. The `truncsum` routine used in [Algorithm A.2](#) is described in [subsection 4.1](#), and the `Cross-DEIM` routine used in [Algorithm 4.5](#) is described in [subsection 4.2](#).

---

**Algorithm A.2** [W-factors, V-factors] = OFT-SqrtInv(W<sub>in</sub>-factors, V<sub>in</sub>-factors, { $\tau_k$ }, { $\omega_k$ },  $\alpha$ ,  $\beta$ ,  $\kappa$ ,  $\epsilon$ )

Low-rank evaluation of  $A^{-1/2}g$  via the OFT integral

---

- 1: **Input:** Initial low-rank factors  $U_W^{(0)}\Sigma_W^{(0)}(V_W^{(0)})^T$ ,  $U_V^{(0)}\Sigma_V^{(0)}(V_V^{(0)})^T$ ; time grid  $\{\tau_k\}_{k=0}^N$ ; quadrature weights  $\{\omega_k\}_{k=0}^N$ ; parameters  $\alpha, \beta, \kappa$ ; tolerance  $\epsilon$
  - 2: **Output:** Accumulated low-rank factors for  $W$  and  $V$  components of  $A^{-1/2}g$
  - 3:  $\omega_r + i\omega_i \leftarrow \omega_0$ ,  $\Delta t_0 \leftarrow \tau_1 - \tau_0$ ,  $\epsilon_0 \leftarrow \Delta t_0^3$  {Initialize accumulator with first quadrature point.}
  - 4:  $[U_V^{\text{acc}}, \Sigma_V^{\text{acc}}, V_V^{\text{acc}}] \leftarrow \text{truncsum}\left(U_V^{(0)}(\omega_r\Sigma_V^{(0)})(V_V^{(0)})^T + U_W^{(0)}(-\omega_i\Sigma_W^{(0)})(V_W^{(0)})^T, \epsilon_0, n\right)$
  - 5:  $[U_W^{\text{acc}}, \Sigma_W^{\text{acc}}, V_W^{\text{acc}}] \leftarrow \text{truncsum}\left(U_V^{(0)}(\omega_i\Sigma_V^{(0)})(V_V^{(0)})^T + U_W^{(0)}(\omega_r\Sigma_W^{(0)})(V_W^{(0)})^T, \epsilon_0, n\right)$
  - 6: **for**  $k = 0, 1, \dots, N - 1$  **do**
  - 7:  $\Delta t_k \leftarrow \tau_{k+1} - \tau_k$ ,  $\epsilon_k \leftarrow \Delta t_k^3$
  - 8:  $[U_W^{(k+1)}, \Sigma_W^{(k+1)}, V_W^{(k+1)}], [U_V^{(k+1)}, \Sigma_V^{(k+1)}, V_V^{(k+1)}] \leftarrow$   
 $\text{LR-Timestep}\left([U_W^{(k)}, \Sigma_W^{(k)}, V_W^{(k)}], [U_V^{(k)}, \Sigma_V^{(k)}, V_V^{(k)}], \{\lambda_j\}, \Delta t_k, \alpha, \beta, \kappa\right)$  {Advance Schrödinger equation one step ([Algorithm 4.5](#)).}
  - 9:  $\omega_r + i\omega_i \leftarrow \omega_{k+1}$  {Accumulate with quadrature weight  $\omega_{k+1}$ .}
  - 10:  $[U_V^{\text{acc}}, \Sigma_V^{\text{acc}}, V_V^{\text{acc}}] \leftarrow \text{truncsum}\left(U_V^{\text{acc}}\Sigma_V^{\text{acc}}(V_V^{\text{acc}})^T + U_V^{(k+1)}(\omega_r\Sigma_V^{(k+1)})(V_V^{(k+1)})^T + U_W^{(k+1)}(-\omega_i\Sigma_W^{(k+1)})(V_W^{(k+1)})^T, \epsilon_0, n\right)$
  - 11:  $[U_W^{\text{acc}}, \Sigma_W^{\text{acc}}, V_W^{\text{acc}}] \leftarrow \text{truncsum}\left(U_W^{\text{acc}}\Sigma_W^{\text{acc}}(V_W^{\text{acc}})^T + U_V^{(k+1)}(\omega_i\Sigma_V^{(k+1)})(V_V^{(k+1)})^T + U_W^{(k+1)}(\omega_r\Sigma_W^{(k+1)})(V_W^{(k+1)})^T, \epsilon_0, n\right)$
  - 12: **end for**
  - 13: **return**  $[U_W^{\text{acc}}, \Sigma_W^{\text{acc}}, V_W^{\text{acc}}], [U_V^{\text{acc}}, \Sigma_V^{\text{acc}}, V_V^{\text{acc}}]$
- 

## REFERENCES

- [1] D. APPELÖ AND Y. CHENG, *lrAA: Low-Rank Anderson Acceleration*, SISC (in-revision), (2025).
- [2] D. APPELÖ AND Y. CHENG, *A new cross approximation for Tucker tensors and its application in Tucker-Anderson acceleration*, Submitted (arXiv:2509.18554), (2025).
- [3] D. APPELÖ, F. GARCIA, AND O. RUNBORG, *WaveHoltz: Iterative solution of the Helmholtz equation via the wave equation*, SIAM Journal on Scientific Computing, 42 (2020), pp. A1950–A1983.
- [4] M. CUBILLOS AND E. JIMENEZ, *A novel direct Helmholtz solver in inhomogeneous media based on the operator Fourier transform functional calculus*, Journal of Computational Physics, 527 (2025), p. 113808.
- [5] J. W. DEMMEL, *Applied Numerical Linear Algebra*, Society for Industrial and Applied Mathematics, 1997, <https://doi.org/10.1137/1.9781611971446>, <https://epubs.siam.org/doi/abs/10.1137/1.9781611971446>, <https://arxiv.org/abs/https://epubs.siam.org/doi/pdf/10.1137/1.9781611971446>.
- [6] P. A. M. DIRAC, *Note on exchange phenomena in the thomas atom*, Mathematical Proceedings of the Cambridge Philosophical Society, 26 (1930), p. 376–385, <https://doi.org/10.1017/S0305004100016108>.

- [7] M. DONELLO, G. PALKAR, M. NADERI, D. DEL REY FERNÁNDEZ, AND H. BABAEI, *Oblique projection for scalable rank-adaptive reduced-order modelling of nonlinear stochastic partial differential equations with time-dependent bases*, Proceedings of the Royal Society A, 479 (2023), p. 20230320.
- [8] Z. DRMAC AND S. GUGERCIN, *A new selection operator for the discrete empirical interpolation method—improved a priori error bound and extensions*, SIAM Journal on Scientific Computing, 38 (2016), pp. A631–A648.
- [9] S. A. GOREINOV, E. E. TYRTYSHNIKOV, AND N. L. ZAMARASHKIN, *A theory of pseudoskeleton approximations*, Linear algebra and its applications, 261 (1997), pp. 1–21.
- [10] A. GRANATH, D. APPELÖ, AND S. WANG, *LR-WaveHoltz: A low-rank helmholtz solver*, 2025, <https://arxiv.org/abs/2510.09352>, <https://arxiv.org/abs/2510.09352>.
- [11] O. KOCH AND C. LUBICH, *Dynamical low-rank approximation*, SIAM Journal on Matrix Analysis and Applications, 29 (2007), pp. 434–454, <https://doi.org/10.1137/050639703>, <https://doi.org/10.1137/050639703>, <https://arxiv.org/abs/https://doi.org/10.1137/050639703>.
- [12] C. LUBICH, *From Quantum to Classical Molecular Dynamics: Reduced Models and Numerical Analysis*, Zurich Lectures in Advanced Mathematics, European Mathematical Society, Zürich, 2008, <https://doi.org/10.4171/067>.
- [13] M. W. MAHONEY AND P. DRINEAS, *CUR matrix decompositions for improved data analysis*, Proceedings of the National Academy of Sciences, 106 (2009), pp. 697–702.
- [14] I. V. OSELEDETS, D. SAVOSTIANOV, AND E. E. TYRTYSHNIKOV, *Tucker dimensionality reduction of three-dimensional arrays in linear time*, SIAM Journal on Matrix Analysis and Applications, 30 (2008), pp. 939–956.
- [15] D. C. SORENSEN AND M. EMBREE, *A DEIM induced cur factorization*, SIAM Journal on Scientific Computing, 38 (2016), pp. A1454–A1482, <https://doi.org/10.1137/140978430>.